Int j simul model 22 (2023) 2, 279-290
Original scientific paper

SIMULATION OF CORROSION IN THE RIVETED ZONE OF ALUMINIUM-BASED SKIN

Niu, L. Q.[*]; Yang, X. B.[**,#]; Si, Q. M.[*]; Li, Z.[*] & Wang, C. Y.[***]
[*] School of Civil Aviation, Zhengzhou University of Aeronautics, Zhengzhou, 450046, China
[**] School of Experimental Technique, Henan Chemical Technician College, Kaifeng, 475000, China
[***] School of Safety Science and Engineering, Henan Polytechnic University, Jiaozuo, 454000, China
E-Mail: yangxbcivil@hotmail.com ([#] Corresponding author)

Abstract
In order to explore the local corrosion mechanism of the riveted zone of aluminium-based skins under coating pre-damage, COMSOL Multiphysics was utilized to simulate a physico-chemical model with the laboratory test results of electrochemical parameters as boundary conditions. The time-domain variation of electrochemical behaviour parameters was analysed, and the dynamic corrosion characteristics in the riveted zone were revealed. Results show that after coating damage, with the simulation time going on from 0 day to 30 days, erosive ions continuously invade, and the corrosion reaction is gradually aggravated in the riveted zone, leading to a growth trend of the electrolytic electrode potential. At 30 days, the thickness of electrode deposits increases by 0.16 μm, and the electrolytic potential distribution ranges from 0.025 V to 0.028 V. By setting the electrolytic ion concentration in the coating pre-damage zone reasonably, the corrosion mechanism and morphology of the riveted zone of aluminium-based skins under different electrolyte concentrations can be explored, which can save laboratory check and verification time as well as improve work efficiency.
(Received in February 2023, accepted in May 2023. This paper was with the authors 5 weeks for 2 revisions.)

Key Words: Aluminium-Based Skin, Corrosion, Coating Pre-Damage

1. INTRODUCTION

Corrosion is a harmful phenomenon leading to the degradation and failure of material structures, which will result in huge economic losses to human beings, often pose safety threats, and cause life dangers [1]. Based on specific failure modes, corrosion exerts influences in different forms, such as uniform corrosion, galvanic corrosion, and crevice corrosion [2]. As a multi-purpose and high-strength material, aluminium alloy has been widely applied in the aerospace field to manufacture high-load parts and components. As the skin of aircrafts, aluminium alloy surrounds the aircraft skeleton structure to form a dimensional component of an aerodynamic shape of the aircraft, which is usually fixed by rivets [3]. Considering the external environment, the corrosion of aircraft skins is nonnegligible, particularly in the riveted zone, which is prone to corrosion failure because such characteristics, including material composition, local cracks, and stress concentration, directly affect the safety and reliability of the aircraft. At present, organic coatings serve as the main protective system of aircraft skin structures, which isolate the direct contact between the substrate and corrosive media and prevent the corrosion of the substrate [4, 5]. Once the coating is damaged, the skin will be exposed to the external environment, which easily results in corrosion.

Current studies regarding coating damage mostly focus on the aging failure of coating, whereas little attention has been paid to the continuous corrosion of the substrate after failure. In practical application, substrate corrosion may occur at the initial stage of coating damage, which is often not easy to detect, and the corrosion of the substrate will aggravate the scope of coating damage. Research on the corrosion of the skin's riveted zone focuses on laboratory examination and verification of riveting components but less on the failure process. In the experiment, most riveting components are not coated on the basis of the actual use, and the

interaction between riveting components and coatings has rarely been explored. Laboratory analysis of the corrosion of the skin's riveted zone relies on a variety of experimental technical means and requires complex instruments and a large number of consumable materials, which leads to high asset and time costs spent on the research process. Considering the abovementioned shortcomings, a corrosion scene of the riveted zone of an aluminium-based skin under coating pre-damage was designed, and the electrolyte potential, electrolyte current density, and ion concentration in the riveted zone at different time steps were compared using the technical method of simulation to reveal the corrosion characteristics of the riveted zone under coating pre-damage. Furthermore, the key spatial–temporal points of corrosion behaviour were proposed to comprehensively improve the prediction and protection level of corrosion in the riveted zone.

2. STATE OF THE ART

With regard to corrosion in the riveted zone of aluminium-based skins, related research focuses on the coating failure and riveting metal corrosion, particularly the coating failure or coating-free riveting metal corrosion [6-8], without considering the corrosion process of riveting metals after the coating failure and the influence of riveting metal corrosion on the coating failure. For example, Tiong and Clark [9] performed finite element modelling and experiments on the general joint structure for representative light military and civil aircraft structures, predicted the displacement at the plate end of the joint under the maximum load capacity, and measured the critical displacement of the coating layer at the interface. Calabrese's research team [10, 11] evaluated the durability behaviour and performance of the self-perforating riveted joint of aluminium alloy plates; determined the shear capacity of the joint through a shear test of the single-lap joint; evaluated the durability of the mechanical joint under key environmental conditions after a long-term aging test; analysed the anode and cathode behaviour of the metal components of the riveted joint through an action potential polarization test; conducted a long-term aging test in the salt spray environment; studied the relationship among the failure mechanism, joint shape, and corrosion damage; and proposed a theoretical model to predict the failure mode. Karim et al. [12] analysed the influence of different rivet coatings on the corrosion behaviour and strength degradation of riveted joints among different materials. Through a 1-week accelerated corrosion test, the corrosion phenomenon and subsequent strength degradation of the joints were studied. Zhang et al. [13] naturally exposed aluminium alloy-riveted structure test pieces in different marine environments. Through comparative analysis of the corrosion of the test pieces after 1 year, the effect of corrosion in marine service environment on aluminium alloy-riveted structures was studied, and the result showed that intact coating could exert a good protective effect on the marine environment. Based on the abovementioned research results, relevant scholars have primarily analysed the coating failure or the corrosion behaviour of metals in the riveted zone through experimental studies, evaluated the corrosion behaviour by instrumental analysis, and then established failure prediction models, which are restricted to laboratory means. However, coatings and metals have been rarely studied simultaneously to explore the interaction between the coating failure and corrosion of riveting components.

In addition, for the numerical simulation of metal corrosion, scholars have carried out simulation of electrochemical corrosion-like metal galvanic corrosion, stress corrosion, and pitting corrosion through the finite element method (FEM) [14, 15]. Prajapati et al. [16] studied the pitting corrosion behaviour in 316 stainless-steel pipelines by COMSOL Multiphysics and discussed the variation trend of electrochemical parameters, such as electrolyte point location and current density, and the number of pitting corrosions. With the gradual maturity of numerical simulation technology and method, the coordination of simulation and corrosion has

become the goal pursued by researchers in the field of corrosion, for example, the coupling simulation of multiple corrosion types and simulation of corrosion after coating damage on the metal surface. In recent years, Chen's research team [17, 18] simulated coupling between mechanical and electrochemical corrosions via COMSOL Multiphysics; proposed a multi-physical field model involving mechanical–electrochemical coupling, anodic dissolution, formation of insoluble deposits, and the resulting galvanic pitting corrosion to study the complex local corrosion process; and revealed the autocatalytic process of pitting corrosion in case of increasing erosion and stress concentration in the chemical environment. Saeedikhani et al. [19] used the moving boundary-time model of COMSOL Multiphysics to simulate the corrosion mechanism of galvanized steel plates with scratches on the surface of the zinc layer, tracked the boundary expansion of the corrosion zone by introducing the Lagrange method, and explored the dynamic morphological change of zinc corrosion. Finite element simulation can make up for the results that cannot be achieved because of experimental conditions, equipment, or aging limitations, and it is an effective method to quantify metal corrosion. Considering the numerical simulation of metal corrosion, the research perspective focuses on the electrochemical corrosion simulation of the metal material but not on the metal material and protective coating as a whole system, which leads to deviation between the simulation results and the actual service process of metal materials as well as limited theoretical support for metal corrosion protection.

Therefore, boundary conditions were set using polarization curve test results, and an ideal model incorporating such composite factors, such as electrochemical field coupling, anodic dissolution, and the formation of insoluble deposits, was established on the basis of the corrosion mechanism and dynamic process. Then, the development of a dynamic corrosion process in the riveted zone under coating pre-damage was discussed by exploring the time-domain changes in the ion concentration, electrolyte potential, and current density, thereby providing a theoretical reference for life prediction and management of in-service components in the riveted zone in the environment and improving the coating maintenance efficiency in the riveted zone.

3. METHODOLOGY AND MODEL

3.1 Polarization curve test method

Polarization curves, which characterize the current density-dependent change of the overpotential and represent the functional relationship between the driving potential of corrosion reaction and the reaction speed current, can describe the trend of metal corrosion damage. In improving the simulation accuracy, the corrosion kinetics parameters (corrosion potential, etc.) were provided for corrosion simulation by using the actual Tafel polarization curve test results. The polarization curve of 2024 aluminium alloy in NaCl solution was tested by electrochemical workstation AUTOLAB PGSTAT 302N, and a corrosion test electrolytic cell composed of three electrodes was adopted, in which aluminium alloy with an effective exposed area of 1 cm^2 was used as the working electrode, Ag/AgCl electrode as the reference electrode, and Pt electrode as the auxiliary electrode. The test temperature was room temperature; the scanning voltage ranged from −0.5 to 0.5 V (vs. OCP), and the scanning speed was 1 mV/s.

3.2 Corrosion simulation

COMSOL Multiphysics, which was developed by Swedish COMSOL Company, is derived from MATLAB's Toolbox module and combined with the multi-physics coupling advantage and outstanding computing power of ANSYS Fluent [20]. In addition, COMSOL can be used

to directly simulate 1D, 2D, and 3D electrochemical corrosion processes; describe electrochemical reaction kinetics through Tafel, Butler–Volmer, or other user-defined equations; simulate time change trends of the corrosion surface and in the nearby electrolyte; and explore the transfer in corrosive substances and materials. In this study, COMSOL Multiphysics was used to achieve the corrosion simulation of the riveted zone of an aluminium-based skin under coating pre-damage.

3.3 Physical model

In this study, 2024 aluminium alloy was selected as the material of aluminium-based skin substrate and rivet, the 3D model of the riveting joint is shown in Fig. 1 a, and a riveted zone was selected as the studied zone in the model. As shown in Fig. 1 b, a microcrack was generated on the surface of the riveted zone. In maintaining the calculation results and simplifying the calculation, the 3D model shown in Fig. 1 was simplified. With the electrolyte infiltrating after coating damage as the studied interface, the rivet and skin substrate were in contact with the electrolyte; the corrosion deformation of the substrate surface with time was discussed, and the model was transformed into a 2D problem of corrosion deformation. In establishing an accurate model and solving it by computer, some assumptions must be made: the chemical and electrochemical reactions considered in the model originated near the damaged zone of the film; the electrolyte zone had a concentration gradient, and the upper interface was a constant value. The layer formed at the interface was only attributed to the formation of $Al(OH)_3$, and it would not dissolve again after formation. The convection process was not taken into account. Considering the transfer of electrolyte ions during the electrochemical reaction, the tertiary current distribution was used to support the establishment of an electrolytic corrosion simulation model, and the corrosion of the riveted zone under coating pre-damage was simulated and analysed using a 2D cross-sectional micromodel. Then, the initialization time dependence of the transient electrochemical problem, including the deforming mesh physical interface in COMSOL Multiphysics, was studied.

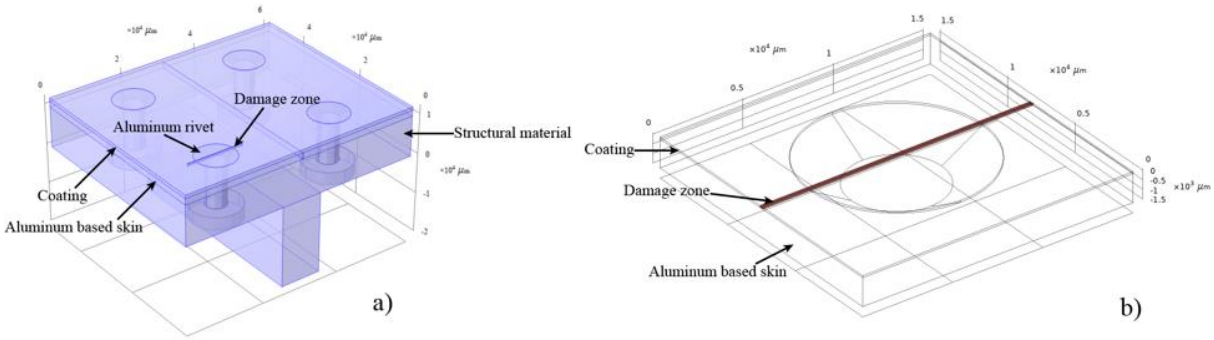

Figure 1: Schematic diagram of the 3D model of aluminium alloy and rivet connection: a) riveting structural parts, b) local enlargement of the riveted zone.

The study was completed in two steps. In the first step, the current distribution was initialized, and the steady-state process was solved using a steady-state equation; in the second step, the steady-state value calculated in the first step was considered as the initial value of time correlation research to solve the transient process of the model. The specific mesh size and mesh generation are shown in Fig. 2. The mesh generation area was a corrosive electrolyte, with a size of 10 μm × 5 μm, and a 1 μm-deep rivet-aluminium substrate-riveting gap was set below. The left and right sides of the electrolyte were connected with the coating; the rivet was directly below the left side, and the aluminium substrate was directly below the right side. The electrolyte was 0.5 mol/L NaCl solution with pH set to 10. In accurately simulating the corrosion process and avoiding losing some related features because of coarse meshes [21], free

triangular meshes were adopted for the model, which was calibrated into a general physics model. The mesh elements were relatively dense and densified in the interfacial zone. The divided complete mesh included 11,117 domain elements and 435 boundary elements.

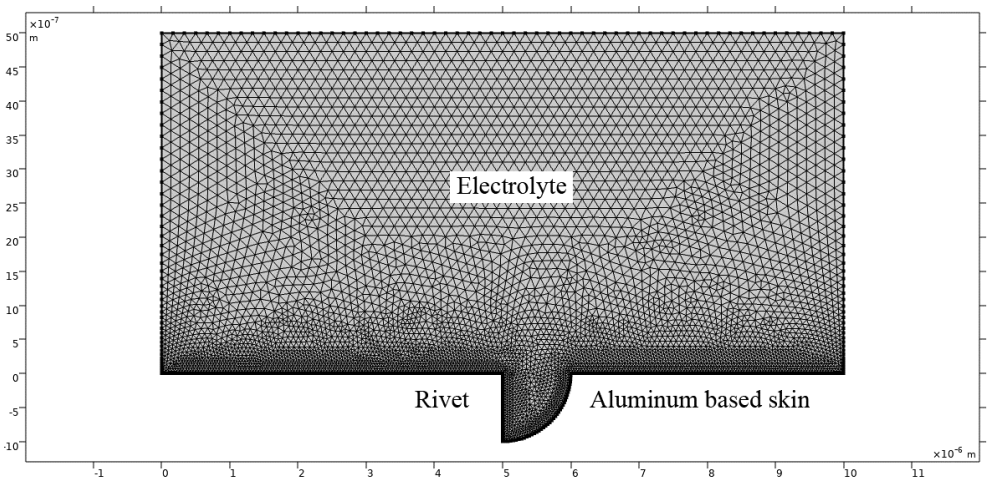

Figure 2: Schematic diagram of mesh generation for the corrosion model.

3.4 Mathematical model

The mathematical model of metal corrosion primarily includes differential governing equations and boundary conditions.

Governing equation: In the electrochemical reaction, the potential difference among electrodes will induce the formation of a corrosive electric field in electrolyte solution. In the state of ideal electrolyte solution, the transport flux of any particle *i* in the electric field is given by Nerst–Planck, which represents the mass transfer of the electrolyte:

$$N_i = -D_i \nabla C_i - Z_i F u_i C_i \nabla \varphi_l + C_i U \tag{1}$$

where N_i is the flux, D_i is the diffusion coefficient, C_i is the concentration of charges, Z_i is the charge number of species *i*, u_i is the bulk velocity, *F* is the Faraday constant, φ_l is the potential of electrolyte, *U* is the solvent velocity and in this study set to be 0.

The general equation used to analyse the transport of substances in electrolyte solution is based on the law of conservation of mass:

$$\frac{\partial C_i}{\partial t} + \nabla \cdot N_i = R_i \tag{2}$$

where R_i represents the rate of accumulation or removal of species *i* via electrochemical reactions.

In simulating the corrosion of the riveted zone and considering the concentration of substances, an appropriate electrochemical reaction should be added to solve the potential and current density of the selected electrode and electrolyte zones. In the model, the riveted zone is a metal conductor, and the relationship between current and voltage follows Ohm's law:

$$i_s = -\sigma_s \nabla \varphi_s \tag{3}$$

In addition, the law of conservation of current is presented as follows:

$$\nabla \cdot i_s = Q_s \tag{4}$$

where i_s represents the current density vector of electrode (A/m^2), σ_s denotes the conductivity (S/m), φ_s is the electric potential in metal conductor (V), and Q_s is the current source term (A/m^3).

An electrolyte is an ionic conductor, and the net current density can be described by the sum of the fluxes of all ions.

$$i_l = F\sum_i z_i N_i \tag{5}$$

The formula of electrolyte current conservation is shown as follows:

$$\nabla \cdot i_l = Q_l \tag{6}$$

where i_l represents the current density vector of electrolyte (A/m^2), and Q_l is the current source term of electrolyte (A/m^3).

The electrolyte charge transfer is measured using the Butler–Volmer equation:

$$i = i_0\left[\exp\left(\frac{\alpha_a n_e F\eta}{RT}\right) - \exp\left(\frac{\alpha_c n_e F\eta}{RT}\right)\right] \tag{7}$$

$$\frac{dn}{dt} = \frac{1}{n_e F} \tag{8}$$

$$\eta = E - E_{eq} \tag{9}$$

where α_a and α_c are the anodic charge and cathodic charge transfer coefficient, respectively, i and i_0 are the electrode and exchange current densities in A/m^2, respectively. n_e is the number of electrons involved in the electrode reaction, η is the activation overpotential, n is the number of moles of species, and E and E_{eq} represent electrode and equilibrium potential in volts, respectively.

Boundary conditions: In this study, 2024 aluminium alloy was used as the anode metal material, and the interface between the film and electrolyte was used as the cathode. In addition, 0.5 mol/L of NaCl solution was set as the electrolyte in the riveted zone. In the Nerst–Planck equation, separate boundary conditions are set for substance concentration and potential, together with two dynamic boundary conditions (substance concentration and potential boundary conditions) on each boundary, and insulation boundary conditions are set as follows:

$$-n \cdot i_l = 0, -n \cdot i_s = 0 \tag{10}$$

where n is the normal vector to the boundary pointing outward and i is the current density.

The electrolyte potential and its initial value were set to 0 V and the electrolyte temperature to 293.15 K. A “dissolved-deposited substance” was added on the anode electrode surface; the density and molar mass of $Al(OH)_3$ were input, and the initial value of the electrolyte potential was set to 0 V at the cathode.

The dissolution reaction of the aluminium substrate took place on the anode surface, whereas the oxygen absorption reaction occurred on the cathode surface. Corrosion parameters (Table I) such as the corrosion current density and electrode potential were obtained through the polarization curve test of 2024 aluminium alloy, which then served as the basic input parameter of the model.

Table I: Electrochemical parameters of the polarization curve of 2024 aluminium alloy.

Sample	φ_{corr} (V) **vs. Ag/AgCl**	i_{corr} (A/cm^2)	b_a (V/dec)	b_c (V/dec)
2024Al	-1.058	1.844×10^{-6}	0.154	0.049

4. RESULT ANALYSIS AND DISCUSSION

4.1 Ion concentration distribution

During metal corrosion, the time-dependent change of the ion concentration in the electrolyte could indicate the reaction at the set coating damage position. In simulating the formation of $Al(OH)_3$ by Al^{3+}, the pH of the electrolyte was set high; thus, OH^- existed in the electrolyte in large quantity. By observing the changes in Al^{3+} and Cl^- during simulation, the corrosion reaction process of the coating damage zone was discussed. The time-dependent change in the

distribution of Al^{3+} concentration is shown in Fig. 3. The concentration was greater at a closer distance to the bottom of the damage zone, indicating that the corrosion effect was more evident than that in other zones. The Al^{3+} ion concentration in the damage zone also increased with time, indicating that corrosion continued, and the generation rate of Al^{3+} was higher than that of $Al(OH)_3$. The concentration distribution of Cl^- obtained by numerical simulation is shown in Fig. 4. A concentration gradient was observed between the riveted zone and electrolyte surface. The closer to the bottom of the damage zone, the greater the concentration. The simulated streamline formed a cycle on the surface of the riveted zone and inside the damage zone, revealing that the local electrochemical reaction was taking place in the riveted zone. The Cl^- concentration in the damage zone increased with time, which was attributed to the deepening of the damage zone and the increase of Al^{3+} generated by the internal corrosion reaction. The distribution of ion concentration and its time-dependent changes revealed the corrosion reaction in the riveted zone under coating pre-damaged to a certain extent. In actual corrosion, the corrosion activity of intermetallic particles may be hindered by the formation of corrosion products; thus, the tested ion concentration is different from the model result.

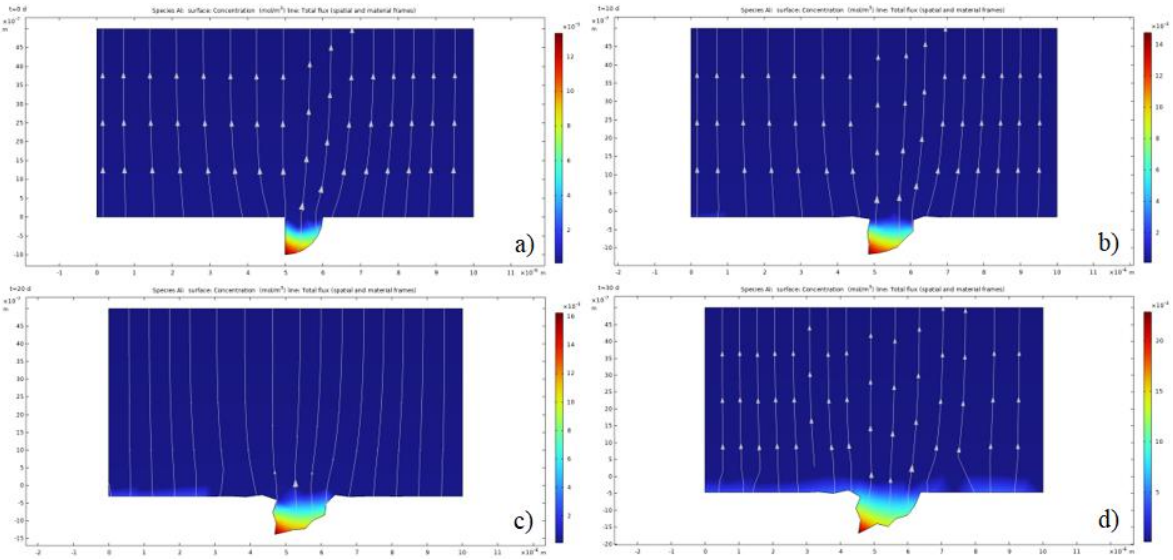

Figure 3: Concentration distribution of Al^{3+}: a) $t = 0$ day, b) $t = 10$ days, c) $t = 20$ days, d) $t = 30$ days.

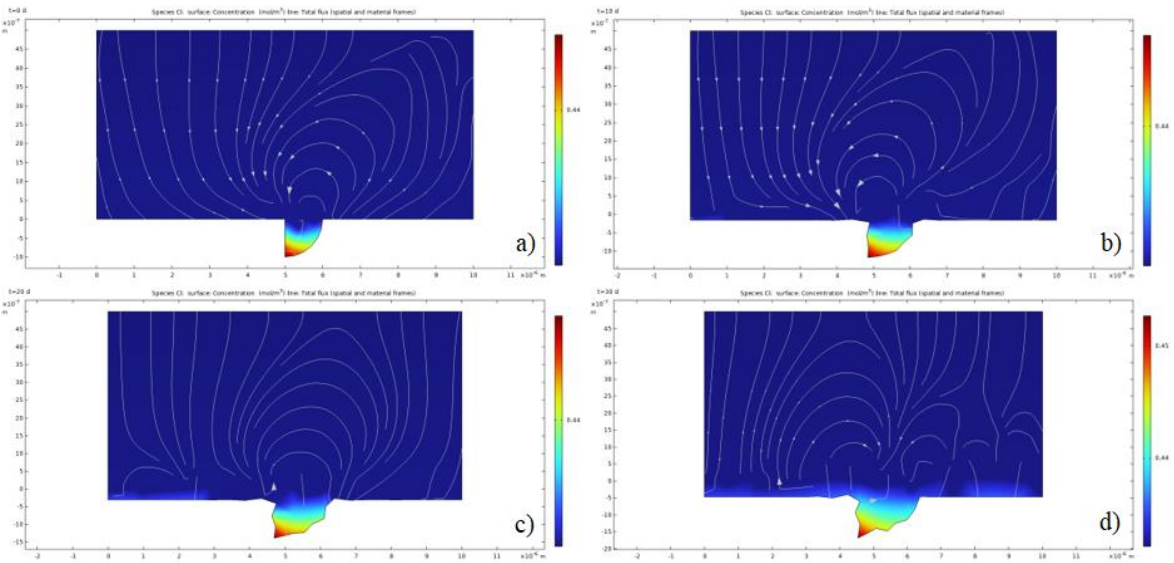

Figure 4: Concentration distribution of Cl^-: a) $t = 0$ day, b) $t = 10$ days, c) $t = 20$ days, d) $t = 30$ days.

4.2 Electrolyte potential

In the established model, based on the abovementioned ion concentration distribution, the riveted zone was used as the anode, and the ion concentration of the electrolyte was greater in this zone, thereby making the surface more susceptible to corrosion. The distribution of electrolyte potential was controlled by the Laplace equation. In the initial state, the electrolyte potential was distributed within 0.02–0.022 V, and the electrolyte potential was the highest at the bottom of the damage zone. The higher the potential value, the more likely the corrosion would occur (Fig. 5). Compared with the ion concentration distribution chart, the higher the ion concentration of the electrolyte, the larger the electrolyte potential value in the red zone of the pit. Moreover, the electrolyte potential value decreased along the pit, which was represented by blue, and the result was consistent with the actual situation. With time, in the final state of modelling, the distribution range of electrolyte potential was 0.025–0.028 V, and the potential value increased compared with that under the initial state, indicating that corrosion continuously increased, which might be ascribed to the increase of corrosion in the damage zone.

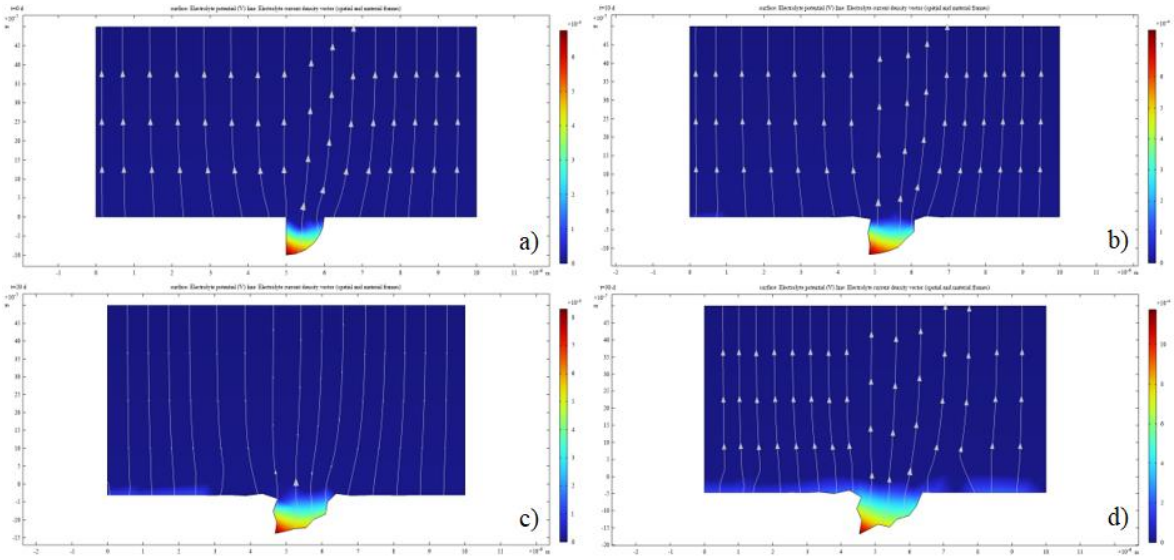

Figure 5: Electrolyte potential change: a) $t = 0$ day, b) $t = 10$ days, c) $t = 20$ days, d) $t = 30$ days.

4.3 Electrolyte current density

In the electrochemical system, anodic and cathodic processes occurred at the interface of electrode and electrolyte simultaneously, and the current density passing through the interface was the product of electron exchange in the two processes. Therefore, the current density distribution played an important role in analysing the corrosion degree of the interface between electrode and electrolyte, which was directly related to the number of transported substances or ions passing through the electrode surface. In addition, the corrosion degree was dependent on the function of electrode dynamics and the material transfer rate, and the higher the current density of the electrolyte, the higher the material dissolution rate in this zone. Based on the obtained simulation data, the damage zone was the most affected zone among all surfaces, and the electrolyte current density was 0.01 A/m^2 (Fig. 6). The electrolyte current density vector shown by the arrow represented the direction of electrons flowing from the anode surface to the cathode, and the current density depended on the number of charge transfer types; thus, the current density in the riveted zone was smaller than that in the damaged pit zone, which was approximately 0.008 A/m^2. With the passage of time to the end of the simulation, the current density in the damaged pit zone slightly increased to 0.012 A/m^2, which might be attributed to the enlargement of the corrosion-induced pit zone despite the increasing number of ions

participating in the reaction. In general, in the simulated period of time, the current density increased in the damaged pit zone and riveted zone. The corrosion in both zones was aggravated, and the change was more evident in the damaged pit zone.

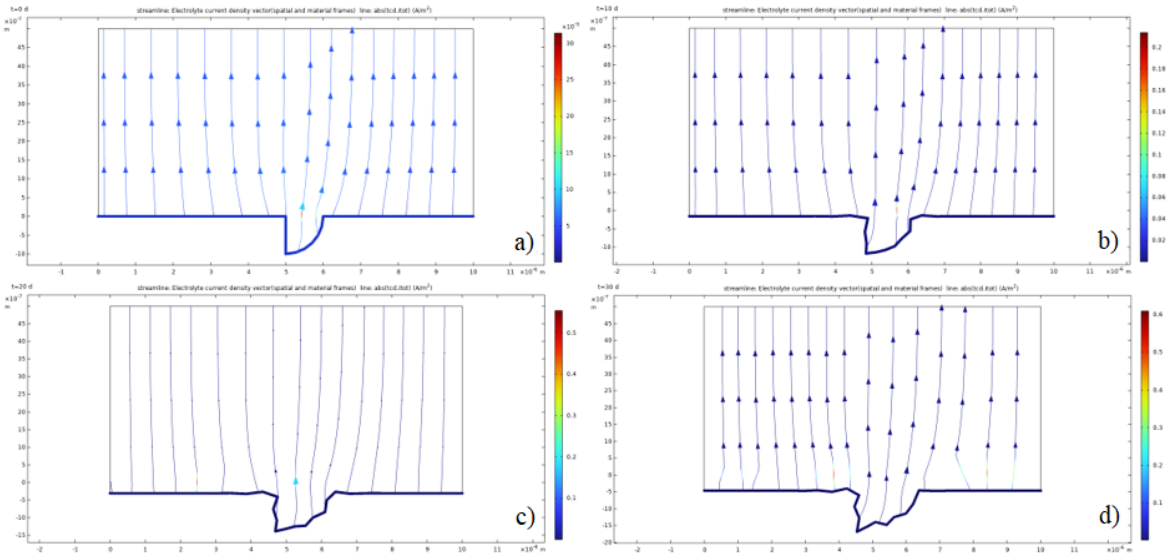

Figure 6: Electrolyte current density change: a) $t = 0$ day, b) $t = 10$ days, c) $t = 20$ days, d) $t = 30$ days.

4.4 Electrode thickness change

When analysing the moving boundary interface, the total thickness of the electrode increased negatively with time, indicating the degradation of surface materials (Fig. 7). On the basis of different colour distributions, the total thickness change of the electrode was displayed. In the final simulation state, the maximum thickness removed was indicated by an orange area, and the minus sign denoted the reduction, which is −1 μm. This finding indicated that the material with a thickness of 1 μm was degraded in the final state.

When analysing the moving boundary surface, surface products were deposited simultaneously, and the thickness of the deposition layer increased with time (Fig. 8). In the final state of simulation, the maximum thickness of deposition was represented by a red area, and its value was approximately 0.16 μm, indicating that the thickness of the deposition layer reached 0.16 μm in the final state.

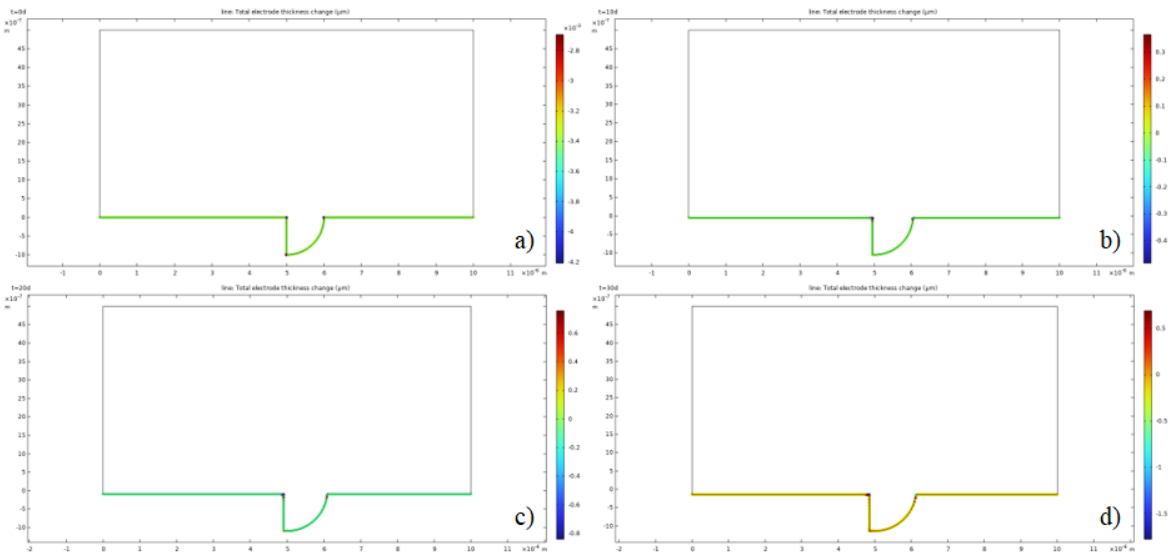

Figure 7: Electrode thickness change: a) $t = 0$ day, b) $t = 10$ days, c) $t = 20$ days, d) $t = 30$ days.

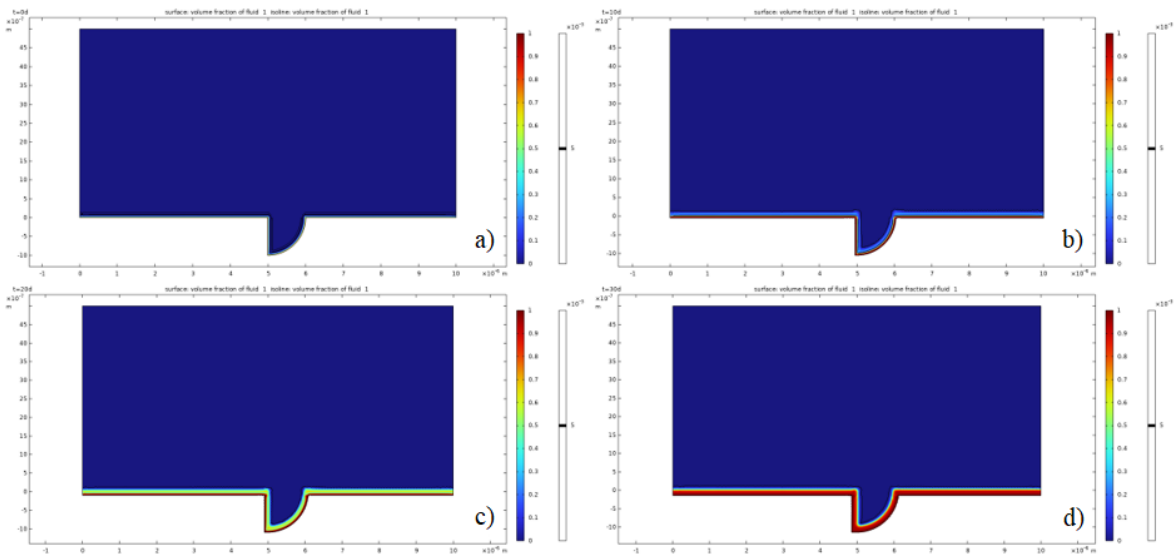

Figure 8: Deposition layer thickness change: a) $t = 0$ day, b) $t = 10$ days, c) $t = 20$ days, d) $t = 30$ days.

5. CONCLUSION

With regard to the corrosion in the riveted zone of an aluminium-based skin under coating pre-damage, a film damage zone in the riveted zone was considered as the study object. Using the theory of corrosion dynamics and the parameters obtained through the polarization curve test of the test aluminium substrate as boundary conditions, the corrosion in the riveted zone of the aluminium-based skin under coating pre-damage was numerically simulated using the tertiary current distribution and geometric deformation module in COMSOL Multiphysics. Then, the dynamic development of corrosion in the riveted zone was discussed by quantitatively analysing the time-dependent variation trends of the following parameters: ion concentration distribution, electrolyte potential, electrolyte current density, electrode potential, and total thickness change of the electrode. Finally, the following conclusions were drawn:

(1) The setting of boundary conditions is the key to corrosion simulation, and the measured values of electrochemical parameters can improve the rationality of boundary condition setting. Using 2024 aluminium substrate as the working electrode, the polarization curve was tested, and the results showed that the self-corrosion potential of the aluminium substrate was −1.058 V; the self-corrosion current was 1.844×10^{-6} A/cm^2; the slope of the anode polarization curve was 0.154 V/dec, and the slope of the cathode polarization curve was 0.049 V/dec.

(2) By simulating the concentration distribution of Al^{3+} and Cl^- near the riveted zone at different time (0, 10, 20, and 30 days), after the coating was damaged, the corrosive ions (Cl^-) showed a positive growth trend in the riveted zone with the extension of time; the corrosion reaction in the riveted zone was intensified with the intrusion of corrosive ions, and the concentration of corrosion products showed a positive growth trend.

(3) By dynamically simulating the time-dependent changes in electrochemical parameters such as electrolyte potential, electrolyte current density, electrode potential, and electrode thickness, as the corrosion reaction proceeded in the riveted zone, the electrolyte potential and current density increased. By 30 days, the electrolyte potential was distributed within 0.025–0.028 V, and the electrolyte current density was 0.012 A/m^2. Meanwhile, the electrode deposit gradually increased to 0.16 μm, and the electrode thickness decreased to 0.15 μm, indicating that the corrosion products gradually diffused beneath the coating, which would affect the bonding effect of the coating and lead to the failure of the coating in the corrosion product area.

COMSOL Multiphysics can be used to quantitatively analyse the time-domain variation trend of corrosion dynamic parameters in the riveted zone caused by coating damage and to

clarify the dynamic corrosion evolution caused by the electrochemical reaction of the anode and cathode as well as the migration, hydrolysis, and precipitation of chemical substances during corrosion in the riveted zone. A geometric model was established under a coating pre-damage scenario, and boundary conditions were set by combining the measured electrochemical parameters. The established model, which was based on actual service conditions, will be of theoretical guiding significance for maintaining the protective coating of aircraft skins in advance, improving the pertinence of maintenance, and reducing the corrosion maintenance cost.

For the model established in this study, relevant boundary parameters were set in accordance with the actual measured data and literature data. However, the actual service environment includes more complicated factors, and the adhesion of the coating affects the deposition of corrosion products, which, to a certain extent, limits the practical application of this model. In the follow-up study, the environmental ion concentration under actual service conditions can be determined in accordance with the service environmental spectra of aircrafts. Meanwhile, a cohesive force model of the film can be added so that the results can be more authentic and persuasive. All the above mentioned results constitute the follow-up research direction.

ACKNOWLEDGEMENTS

This study was supported by the Science and technology planning project of Henan Province in China (No. 232102320049).

REFERENCES

[1] Nazari, M. H.; Zhang, Y.; Mahmoodi, A.; Xu, G.; Yu, J.; Wu, J.; Shi, X. (2022). Nanocomposite organic coatings for corrosion protection of metals: a review of recent advances, *Progress in Organic Coatings*, Vol. 162, Paper 106573, 28 pages, doi:10.1016/j.porgcoat.2021.106573

[2] Shankar, A. R.; Sole, R.; Thyagarajan, K.; George, R. P.; Mudali, U. K. (2019). Failure analysis of titanium heater tubes and stainless steel heat exchanger weld joints in nitric acid loop, *Engineering Failure Analysis*, Vol. 99, 248-262, doi:10.1016/j.engfailanal.2019.02.016

[3] Guo, X. Y.; Zeng, Z.; Li, M. X.; Fu, S. (2022). Simulation of aircraft cabin evacuation strategy based on exit flow equilibrium, *International Journal of Simulation Modelling*, Vol. 21, No. 2, 261-272, doi:10.2507/IJSIMM21-2-601

[4] Zhang, F.; Ju, P.; Pan, M.; Zhang, D.; Huang, Y.; Li, G.; Li, X. (2018). Self-healing mechanisms in smart protective coatings: a review, *Corrosion Science*, Vol. 144, 74-88, doi:10.1016/j.corsci.2018.08.005

[5] Zhang, H.; Zhou, H.; Yang, J.; Song, Y.; Zhao, L. (2019). Synergism of modified graphene oxide to aircraft structural corrosion inhibiting compounds coatings, *Progress in Organic Coatings*, Vol. 132, 490-498, doi:10.1016/j.porgcoat.2019.04.007

[6] Reynolds, L. B.; Twite, R.; Khobaib, M.; Donley, M. S.; Bierwagen, G. P. (1997). Preliminary evaluation of the anticorrosive properties of aircraft coatings by electrochemical methods, *Progress in Organic Coatings*, Vol. 32, No. 1-4, 31-34, doi:10.1016/S0300-9440(97)00098-2

[7] Raps, D.; Hack, T.; Wehr, J.; Zheludkevich, M. L.; Bastos, A. C.; Ferreira, M. G. S.; Nuyken, O. (2009). Electrochemical study of inhibitor-containing organic-inorganic hybrid coatings on AA2024, *Corrosion Science*, Vol. 51, No. 5, 1012-1021, doi:10.1016/j.corsci.2009.02.018

[8] Yang, X. F.; Li, J.; Croll, S. G.; Tallman, D. E.; Bierwagen, G. P. (2003). Degradation of low gloss polyurethane aircraft coatings under UV and prohesion alternating exposures, *Polymer Degradation and Stability*, Vol. 80, No. 1, 51-58, doi:10.1016/S0141-3910(02)00382-8

[9] Tiong, U.; Clark, G. (2011). The structural environment as a factor affecting coating failure in aircraft joints, *Procedia Engineering*, Vol. 2, No. 1, 1393-1401, doi:10.1016/j.proeng.2010.03.151

[10] Calabrese, L.; Bonaccorsi, L.; Proverbio, E.; di Bella, G.; Borsellino, C. (2013). Durability on alternate immersion test of self-piercing riveting aluminium joint, *Materials & Design*, Vol. 46, 849-856, doi:10.1016/j.matdes.2012.11.016

[11] Calabrese, L.; Proverbio, E.; Pollicino, E.; Galtieri, G.; Borsellino, C. (2015). Effect of galvanic corrosion on durability of aluminium/steel self-piercing rivet joints, *Corrosion Engineering, Science and Technology*, Vol. 50, No. 1, 10-17, doi:10.1179/1743278214Y.0000000168

[12] Karim, M. A.; Bae, J. H.; Kam, D. H.; Kim, C.; Choi, W. H.; Park, Y. D. (2020). Assessment of rivet coating corrosion effect on strength degradation of CFRP/aluminium self-piercing riveted joints, *Surface and Coatings Technology*, Vol. 393, Paper 125726, 12 pages, doi:10.1016/j.surfcoat.2020.125726

[13] Zhang, T.; Wang, D.; Li, X.; Li, Y. (2020). Comparative study on corrosion behavior of 7B04 aluminium alloy riveted structure under different sea areas, *Mechanical Science and Technology for Aerospace Engineering*, Vol. 39, No. 8, 1283-1287, doi:10.13433/j.cnki.1003-8728.20190259

[14] Marshall, R. S.; Kelly, R. G.; Goff, A.; Sprinkle, C. (2019). Galvanic corrosion between coated Al alloy plate and stainless steel fasteners, Part 1: FEM model development and validation, *Corrosion*, Vol. 75, No. 12, 1461-1473, doi:10.5006/3308

[15] Mandel, M.; Krüger, L. (2013). Determination of pitting sensitivity of the aluminium alloy EN AW-6060-T6 in a carbon-fibre reinforced plastic/aluminium rivet joint by finite element simulation of the galvanic corrosion process, *Corrosion Science*, Vol. 73, 172-180, doi:10.1016/j.corsci.2013.03.033

[16] Prajapati, V.; Kumar, Y.; Gupta, D.; Kalam, A.; Dubey, M. (2022). Analysis of pitting corrosion of pipelines in a marine corrosive environment using COMSOL Multiphysics, *Journal of Bio- and Tribo-Corrosion*, Vol. 8, Paper 21, 11 pages, doi:10.1007/s40735-021-00620-6

[17] Chen, L.; Ruan, H. (2020). Multi-phase-field modeling of localized corrosion involving galvanic pitting and mechano-electrochemical coupling, *Corrosion Science*, Vol. 177, Paper 108900, 17 pages, doi:10.1016/j.corsci.2020.108900

[18] Chen, L.; Ruan, H.; Shi, S.-Q. (2019). Phase field study of mechanico-electrochemical corrosion, *Electrochimica Acta*, Vol. 310, 240-255, doi:10.1016/j.electacta.2019.04.076

[19] Saeedikhani, M.; Wijesinghe, S.; Blackwood, D. J. (2020). Moving boundary simulation and mechanistic studies of the electrochemical corrosion protection by a damaged zinc coating, *Corrosion Science*, Vol. 163, Paper 108296, 13 pages, doi:10.1016/j.corsci.2019.108296

[20] Dickinson, E. J. F.; Ekström, H.; Fontes, E. (2014). COMSOL Multiphysics®: Finite element software for electrochemical analysis. A mini-review, *Electrochemistry Communications*, Vol. 40, 71-74, doi:10.1016/j.elecom.2013.12.020

[21] Fu, S.; Guo, X. Y.; Dong, L. H.; Sheng, K.; Sun, A. (2022). Numerical simulation of migration laws of dense particle flow in pipelines, *International Journal of Simulation Modelling*, Vol. 21, No. 1, 89-100, doi:10.2507/IJSIMM21-1-592